Minerals Engineering 98 (2016) 52–59

Contents lists available at ScienceDirect

Minerals Engineering

journal homepage: www.elsevier.com/locate/mineng

Textural image classification of foams based on variographic analysis

D. Mesa, W. Kracht *, G. Díaz

Department of Mining Engineering, Universidad de Chile, Chile
Advanced Mining Technology Center, AMTC, Universidad de Chile, Chile

ARTICLE INFO

Article history:
Received 12 February 2016
Revised 22 May 2016
Accepted 27 July 2016
Available online 2 August 2016

Keywords:
Foam
Frothers
Foam texture
Classification

ABSTRACT

Froths can be characterised according to several features, such as colour, bubble size distribution, velocity, mobility or texture. In the case of texture, there are some alternatives that can be used to analyse and classify them, like the texture spectrum analysis, the grey-level co-occurrence matrix, or the wavelet texture analysis. In this work, a variogram-based technique is introduced. Variograms are a widely used geostatistical technique to describe the degree of spatial dependence between sample values as separation between them increases, and have been used before to analyse textures in applications that range from microscopy to satellite images. The purpose of the current work is to introduce the variogram-based technique to compare and classify foams (water-air froths) according to their texture, and studying the effect of frother type on the texture of foams generated in a quasi-2D cell and in a laboratory column. In the case of the quasi-2D foams, the variogram-based textural classification algorithm was able to classify foam images according to the frother used, with an accuracy of 88.9%. In the case of the foam images generated in the laboratory column, the results suggest that foam texture is mainly defined by froth type, with some effect of foam height. The column foam images did not show similar characteristics when grouped by foam gas holdup, which was confirmed with the variogram-based textural analysis.

1. Introduction

It is well known that froth behaviour has a strong impact on flotation (Barbian et al., 2005; Tsatouhas et al., 2006; Hadler and Cilliers, 2009). Froth features such as froth colour, bubble size, froth velocity and froth texture can be used to classify froths in order to develop appropriate flotation control strategies for each type. The froth classification, which may appear simple for an experienced operator, may be difficult for automated systems, and requires good imaging instruments and adequate image analysis techniques.

There are different ways of characterising froth images. They can be characterised by colour and/or by applying morphological algorithms to determine bubble size and shape (Bonifazi et al., 2001), which can be considered physically meaningful features (Aldrich et al., 2010); however, this information may not be descriptive enough to consider the possible spatial distribution of the image components, and froth texture.

1.1. Texture

Texture is usually perceived as related to the properties that a certain area has, usually associated with perceptions such as roughness, smoothness, directionality, among others. Extrapolating to image processing, this concept is related to the perception of an object, or surface, and its description of local variability (Tuceryan and Jain, 1998). Since texture is a local feature that describes the arrangement or structure in a specific area, it can be considered as an important characteristic that could be used to compare and classify froths or foams, which is the objective of this work.

Some alternatives to analyse and classify froth texture are the textures spectrum analysis (Holtham and Nguyen, 2002), the Grey-Level Co-occurrence Matrix (GLCM) (Moolman et al., 1995b,a) and the Wavelet Texture Analysis (WTA) (Bartolacci et al., 2006). In the current work, the use of a variogram-based technique is introduced, which is an alternative method to the co-occurrence matrix for classifying image textures (Carr and De Miranda, 1998).

1.2. Geostatistics and image analysis

The variogram, a widely used geostatistcal technique, is a two-point statistical function that describes the degree of spatial

* Corresponding author at: Department of Mining Engineering, Universidad de Chile, Av. Tupper 2069, Santiago, Chile.
E-mail address: wkracht@ing.uchile.cl (W. Kracht).

http://dx.doi.org/10.1016/j.mineng.2016.07.012
0892-6875/

dependence between sample values as separation between them increases. It characterises the spatial continuity or roughness of a data set, elements in an image for instance, and allows identifying differences that common descriptive statistics and histograms cannot (Barnes, 2003). The variogram in particular, and geostatistics in general, are nowadays frequently applied image processing techniques.

This is not the first time that two-point statistics is used to characterise images related to flotation. Previously, Emery et al. (2012) and Kracht et al. (2013) had used a geostatistical approach to estimate the bubble size distribution of bubbles generated at a laboratory flotation cell, which proved to be a good solution to the problem of sizing bubbles that appear touching each other or overlapping (clusters) in the images.

As shown by Woodcock et al. (1988a,b), variogram characteristics such as height, range and shape, relate to the spatial variation in images. This spatial information can provide data on texture that can be used for classification (Atkinson and Lewis, 2000). Different uses of variogram-based texture analysis are reported in the literature, ranging from microscope to satellite images. Bonetto and Ladaga (1998), for instance, used the variogram method to characterise the texture of scanning electron microscope (SEM) images; Chica-Olmo and Abarca-Hernandez (2000) used geostatistical texture analysis to classify lithologies; Wu et al. (2006) used variogram-based texture analysis to classify urban land-use from aerial images; Jakomulska and Clarke (2001) used variogram-based measures to discriminate between vegetation classes from aerial images; and Fotsing et al. (2013) used variograms to characterise and classify satellite images.

The purpose of the current work is to introduce a variogram-based technique to compare and classify foams according to their texture, and studying the effect of frother type on the texture of foams generated in a quasi-2D cell and in a laboratory column.

2. Experimental

The foam images used in this work were generated from two separate, independent experimental campaigns, the first one performed in a quasi-2D cell, where the images generated correspond to vertical sections of the foam (Fig. 1, left); and the second one performed in a laboratory flotation column, where the foam images correspond to the top of the foam (Fig. 1, right).

2.1. Reagents

The reagents used in this study were: MIBC, Octanol, Oreprep F549, DF250 and PEG300. The composition and supplier of the reagents are summarised in Table 1.

2.2. Quasi-2D cell

A narrow quasi-2D cell was designed in order to study the foam structure. It consisted of an acrylic cell of 20 cm height, 15 cm wide and 1 cm depth, as shown in Fig. 2.

Table 1
Reagents used.

Frother	Characteristics	
MIBC	Composition Supplier	4-Methyl 2-Pentanol ⩾ 98% Sigma Aldrich
Octanol	Composition Supplier	Octanol ⩾ 99% Sigma Aldrich
Oreprep F549	Composition Supplier	Polyglycols (DF250 simile) Cytec Chile
DF250	Composition Supplier	Polyglycols Dow Canada
PEG300	Composition Supplier	Polyethylene glycol ⩾ 99% Sigma Aldrich

A slot sparger, similar to the one proposed by Li et al. (1994), was used for air dispersion. It consists of a system that injects air through a long and narrow slot located at the bottom of the cell, generating a discrete arrangement of equidistant bubble nodes. The slot sparger was built using acrylic and a 100 μm thick stainless steel strip. The gas flow rate was measured with an Omega mass flow meter, FMA1820, and controlled with a rotameter Dwyer, combined with a manometer Festo.

2.3. Laboratory column

The column tests were performed in a Plexiglass laboratory column of 4 m height and 10.16 cm internal diameter with a porous sparger for air dispersion. The column was equipped with a mass flow meter MKS (0–20 L/min) to measure and control the gas flow rate, a differential pressure cell (Bailey) that allows the gas holdup in the collection zone (ε_g) to be calculated, and a conductivity meter, to estimate the foam gas holdup ($\widehat{\varepsilon}_{gf}$) at the top of the column. The foam height was controlled by adding water to the column with a pump. The foam images were captured at the top of the foam (foam surface) as represented schematically in Fig. 3.

2.4. Variogram-based textural classification

2.4.1. Image database

The images in both sets of experiments where taken with the same controlled light (two LED spotlights of 50 W each). This white light was significantly brilliant, in order to overcome any other difference in ambient light. Moreover, all the experiences were performed in a laboratory without direct sunlight.

The original pictures were centred cropped in order to avoid edge lighting variations. Original size of the images for the quasi-2D experiment was 4280 × 2840 pixels and they were cropped to 3250 × 1700. In the case of the column experiments, the original size of the images was 5180 × 3450 and they were cropped to 3900 × 2600.

Figs. 4 and 5 show sample images of these two databases.

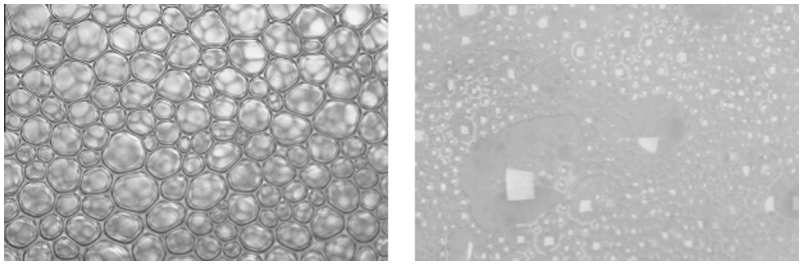

Fig. 1. Example of foam images generated in a quasi-2D cell (left) and in a laboratory flotation column (right). Images not at scale.

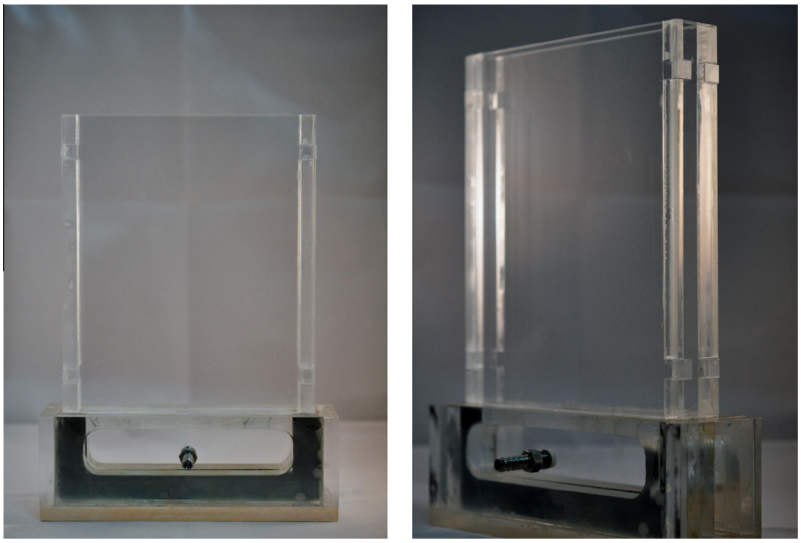

Fig. 2. Quasi-2D cell with a slot sparger.

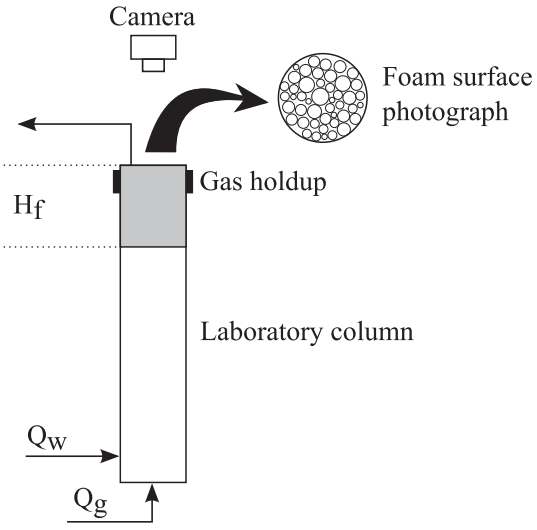

Fig. 3. Laboratory column setup.

The use of different frothers to generate images in both the quasi-2D cell and laboratory column generates foam images with particular bubble separation, shape and arrangements. In both cases the image characteristics suggest variations in the foam texture when different frothers are used.

2.4.2. Textural classification algorithm

An algorithm was developed to compare and classify different foam images according to their texture. In order to extract the structure information of the image, a variographic map is calculated, which is a widely used tool in the field of geostatistics to analyse the spatial behaviour of a variable Deutsch and Journel (1997). The algorithm is intended to capture the main spatial features of the images in order to discriminate information for classification.

The definition of the experimental variogram, which is employed here as the image feature to characterise the foam texture, is presented in Eq. (1):

$$\gamma(h) = \frac{1}{2N(h)} \sum_{k=1}^{N(h)} (Z(x_k) - Z(x_k + h))^2 \quad (1)$$

where $h \in \Re^2$ is a vector that represents the distance used to analyse the variability in the data or lag distance, $N(h)$ is the number of pairs of points to consider for that lag distance and $Z(x_k)$ is the value of the image Z, which correspond to the pixel intensity at position x_k. The matrix containing the variogram information for different lag vectors h is called variographic map.

For an adequate comparison of the variographic maps, they are normalised by dividing each one by its maximum value. With this, all the variographic maps have the same range values. Then, to perform a comparison between the variograhic maps of each foam image, the Mean Square Error (MSE) metric is used, which is presented in Eq. (2):

$$MSE(X, Y) = \sqrt{\sum_{k=1}^{N} (X_k - Y_k)^2} \quad (2)$$

where X and Y are variographic maps to be compared.

The procedure for comparing and classifying foams corresponding to different classes, e.g., generated with different frother types,

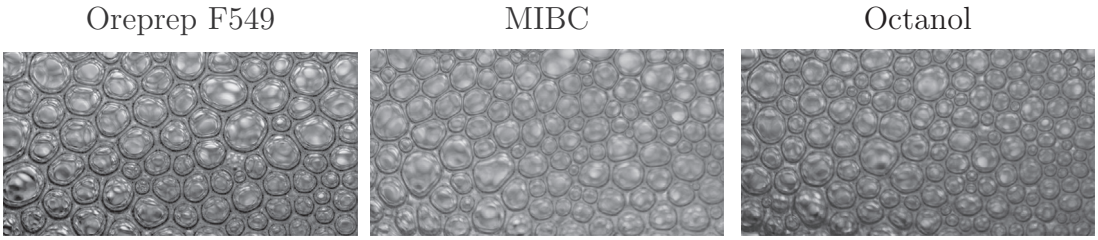

Fig. 4. Sample images from the quasi-2D experiment according to each frother agent used.

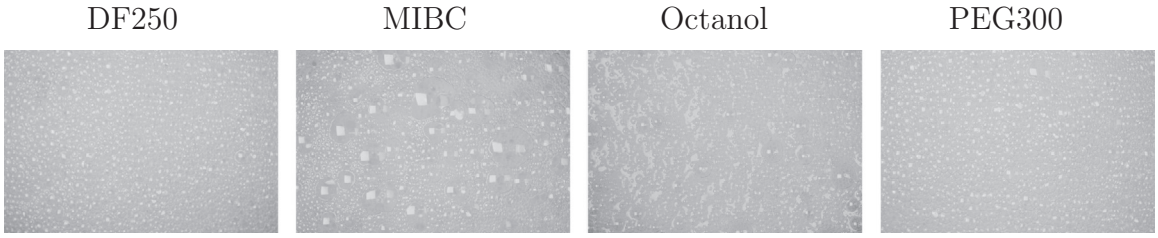

Fig. 5. Sample images from the column experience according to each frother agent used.

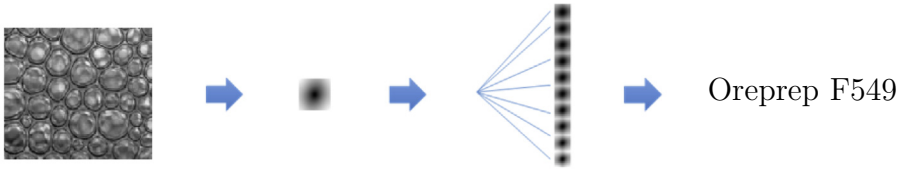

Fig. 6. General scheme of the classification process using the variogram map method.

is as follows: first, the variographic map of an image in the database is calculated. Then, this map is compared against every other map in the database, using MSE metric. Finally, the predicted class corresponds to that of the nearest variographic map (minimum MSE) is obtained as shown in Fig. 6.

The result of applying the algorithm is expressed in a square matrix of $n \times n$, where n is the number of classes tested. This is known as the confusion matrix (see Fig. 7). Rows correspond to the actual class (e.g., frother type) of each image, while columns correspond to where the image is classified by the algorithm.

Fig. 7 shows an example of a confusion matrix where a total of 164 images, corresponding to three classes, are compared and classified. In the example, there are 75 images of Class A, of which 73 are well classified and 2 are misclassified in Class B; from the 54 images corresponding to Class B, 50 are well classified, whereas 1 is misclassified as A, and 3 as C; finally, the 35 images corresponding to Class C are well classified. The accuracy of the classification process can be calculated as the sum of images well classified, i.e., the values in the diagonal of the confusion matrix, divided by the total number of images tested, as expressed in Eq. (3).

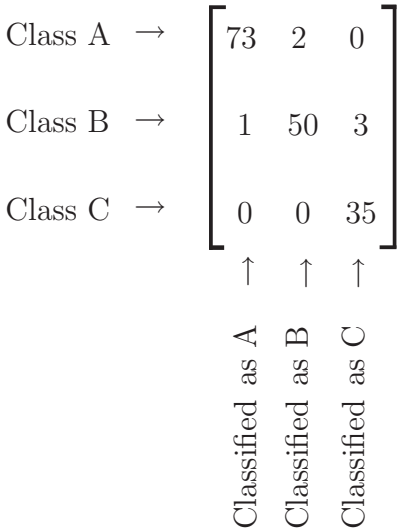

Fig. 7. Example of confusion matrix.

$$Accuracy = \frac{\sum_{i=1}^{n} a_{i,i}}{\sum_{i,j=1}^{n} a_{i,j}} \cdot 100\% \quad (3)$$

where $a_{i,j}$ is the component i,j of the confusion matrix.

In the case of the example presented in Fig. 7, the classification accuracy is 96.3% (158 images well classified over a total of 164 images). A perfect classification would result in a diagonal matrix, with a classification accuracy of 100%.

Texture classifiers require that the homogenous region of each class in the image are large enough, so that the variogram can be computed up to a reasonable number of lags (Atkinson and Lewis, 2000). In the current work this is not an issue because the technique here is applied to compare and classify textures between images, therefore, in this case the region of each class corresponds to the entire image.

3. Results and discussion

3.1. Quasi-2D foams

Three frothers were used in the 2D experimental campaign: Oreprep F549, MIBC and Octanol, at a concentration of 100 ppm. The system was characterised by running tests at J_g = 2.0, 2.5, 3.0 and 3.5 cm/s. For each superficial gas velocity, the equilibrium foam height ($H_{f,eq}$) was recorded in order to generate the $J_g - H_{f,eq}$ curves presented in Fig. 8.

At the highest J_g both Octanol and Oreprep F549 presented foam overflowing; therefore, at this condition it was not possible to determine their equilibrium foam height. This explains why the only value of $H_{f,eq}$ reported at $J_g = 3.5$ cm/s in Fig. 8 corresponds to MIBC.

The $J_g - H_{f,eq}$ curves were used to select a condition at which the three frothers generate roughly the same equilibrium foam height, and there is enough foam in the cell to capture images. At J_g = 2.5 cm/s and foam height $H_{f,eq} \sim 4$ cm the three frothers generated roughly the same equilibrium foam height. The quasi-2D foam images were taken at this condition.

Prior to applying the variogram-based textural analysis, all the images were analysed in the classical way to determine foam bubble size distribution, which are presented in Fig. 9.

As it can be seen in Fig. 9, there is not a significant variation in the bubble size distributions generated at J_g = 2.5 cm/s for the

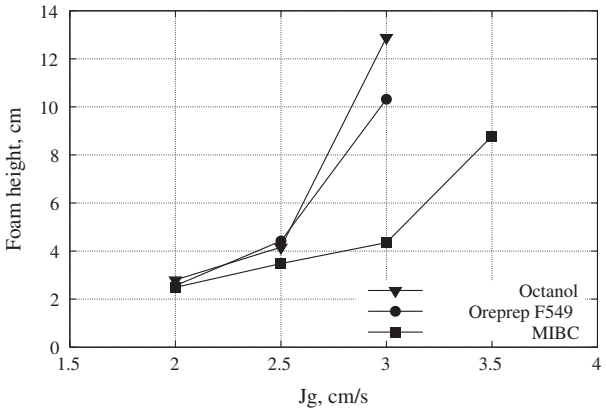

Fig. 8. Equilibrium foam height vs superficial gas velocity in the quasi-2D cell.

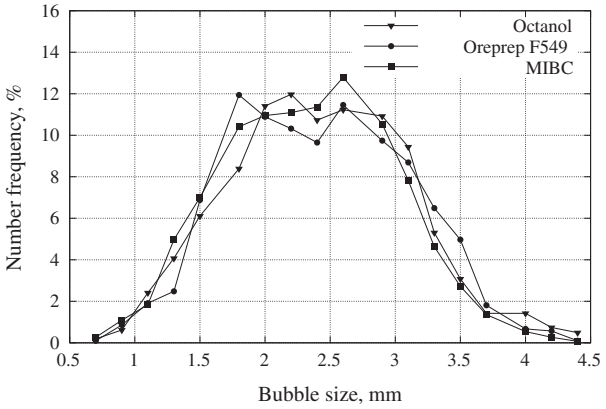

Fig. 9. Foam bubble size distributions generated in a quasi-2D cell at J_g = 2.5 cm/s.

three frothers tested. Therefore, the classical image analysis and the bubble size distribution do not allow the identification of differences between the foams generated with these frothers.

3.2. Textural analysis of quasi-2D foams

The same images analysed for foam bubble size distribution were processed using the variogram-based textural analysis algorithm. For this purpose, a variographic map with a 50 pixels radius was considered, obtaining the confusion matrix shown in Table 2. Since the only difference between foams is the frother type, the classes defined for comparison and classification correspond to the three reagents used: Oreprep F549, MIBC and Octanol.

The classification accuracy is high, with a value of 88.9%. With this result it is possible to say that, even though the bubble size distributions presented in Fig. 9 are the same for the three reagents used, the textures of the quasi-2D foams generated with Oreprep F549, MIBC and Octanol, are recognised as different by the variogram-based textural classification algorithm. Note that this proves that images can be classified according to their texture, but does not allow an absolute measure of the texture to be defined, which in not an objective of this work.

Table 2
Confusion matrix for quasi-2D foams.

	Confusion matrix
DF250	$\begin{bmatrix} 22 & 4 & 1 \\ 2 & 24 & 1 \\ 0 & 1 & 26 \end{bmatrix}$
MIBC	
PEG300	
	Classification accuracy: 95.9%

3.3. Column foams

Four frothers were used in the laboratory column experimental campaign: DF250, MIBC, Octanol, and PEG300. The reagent concentration and the operational conditions of the column were defined in order to have a similar gas dispersion in the collection zone for all the frothers used. This means having the same bubble size (d_{32}), superficial gas velocity (J_g), and gas holdup (ε_g). First, the frothers were characterised and their CCC_{95} was determined, which corresponds to the frother concentration giving a 95% of the size reduction in d_{32} (Finch et al., 2008). A 100% of size reduction due to frother addition corresponds to the difference between d_{32} generated without frother and d_{32} generated at a frother concentration above *CCC*. CCC_{95} corresponds, therefore, to the frother concentration at which a 95% of that size reduction is achieved. At these concentrations, all the frothers produce a similar mean bubble size, $d_{32} \sim 0.83$ mm. After that, the system was characterised, and curves $J_g - \varepsilon_g$ were generated for all the frothers, at concentrations higher than the CCC_{95}, with the purpose of finding a frother concentration C^*, higher than CCC_{95}, at which both J_g and ε_g coincide for all the frothers. Those concentrations are shown in Table 3, along with the values of CCC_{95} determined for each frother.

The gas dispersion conditions in the collection zone, for each frother at concentration C^*, were: $J_g = 0.75$ cm/s, $\varepsilon_g = 15\%$, and bubble surface area flux S_b = 54 s^{-1}. A series of tests was performed at these conditions in the column, but varying the foam height H_f from ~16 cm, which was the minimum foam height at which the foam gas holdup could be measured, until the maximum foam height achievable with each frother. The results of $\hat{\varepsilon}_{gf}$ vs foam height H_f are presented in Fig. 10. The trend line included does not represent any model and is there only as a reference.

For each data point in Fig. 10, a series of images of the top of the foam was captured for textural analysis and classification. Note that the higher the value of H_f the higher the foam gas holdup,

Table 3
Frother concentrations used in the column tests.

Frother	CCC_{95}, ppm	C^*, ppm
DF250	20	35
MIBC	12	80
Octanol	10	25
PEG300	79	150

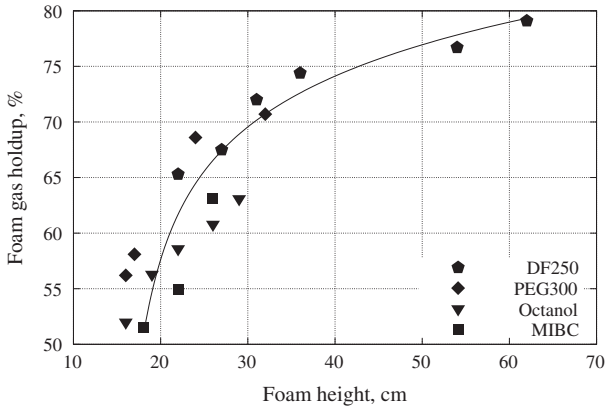

Fig. 10. Foam gas holdup $\hat{\varepsilon}_{gf}$ vs foam height H_f.

which is in agreement with the bubble coalescence and liquid drainage phenomena expected to occur in the foam. Besides that, there is an important difference between the maximum foam height for MIBC ($H_{f,max}$ = 26 cm) and DF250 ($H_{f,max}$ = 62 cm), which was also expected since MIBC is considered a weak frother that generates froths/foams less stable than DF250, considered a strong frother.

3.4. Textural analysis of column foams

In this case, the foam images can be grouped in three different sets of classes: by frother type, foam height and foam gas holdup. Table 4 shows the results of comparing and classifying the foam pictures according to the reagent used.

The classification accuracy is high, with an error lower than 5%. The results, in this case, may be showing that within each class there are images share texture, for example images corresponding to the same condition of frother and foam height, but not necessarily that all the images in the class have the same texture. Therefore, it is of interest to perform the classification but excluding the images generated under the same conditions in the step of comparison. In this way, for instance, in order to classify a foam image corresponding to DF250, at H_f = 31 cm, in the class of DF250, its texture has to be close enough to the texture generated with DF250, but at any other foam height.

Table 5 shows the results of comparing and classifying the foam pictures according to the reagent used, but excluding the images generated under the same conditions of frother type and foam height from the comparison.

The classification accuracy drops from 95.9% to 67.2% when comparing the results of Tables 4 and 5. This means that foam height has some effect on texture, even if the same frother is used. It can be seen from Table 5 that the most important contribution to the drop in classification accuracy is given by the misclassification of PEG300, a polyethylene glycol that is not commonly used as a frother, because it is considered too weak, which is confirmed from the values of CCC_{95} presented in Table 3. According to the results, PEG300 is the frother that presents the strongest effect of foam height on texture. If PEG300 was excluded from the comparison and classification, the accuracy would increase to at least 75%. This is the value that results when the classification accuracy is calculated without considering the numbers of the last row in the confusion matrix presented in Table 5. The actual classification accuracy, excluding PEG300, might be even higher since some of the images misclassified as PEG300 could be well classified if this reagent was not considered.

As mentioned before, the foam images can be grouped not only by frother type, but also by foam height or foam gas holdup. The definition of classes according to foam height, H_f, is presented in Table 6.

The images here are assigned to different classes according to the foam height, without taking into account the frother type. With this, as shown in Table 6, there will be different frothers in each class. The result of comparing and classifying the foam images according to foam height is presented in Table 7. For the reasons explained above, the images generated under the same conditions of foam height and frother type were excluded from the comparison, which means that in order to classify an image generated, for instance, with MIBC at $H_f = 26$ cm as belonging to Class H_f: 26–29 cm, its texture has to be close enough to either Octanol (26–29 cm) or DF250 (27 cm).

The results presented in Table 7 shows a low classification accuracy (23.4%), suggesting that the foam texture is not defined by foam height, and frother effect is far more important, as shown in Table 5. This was expected since the characteristics of the foam should depend not only on the absolute value of foam height, but

Table 4
Confusion matrix for column foams considering frother type.

	Confusion matrix			
DF250	149	0	0	5
MIBC	0	66	0	0
Octanol	0	0	105	5
PEG300	7	0	0	81

Classification accuracy: 95.9%

Table 5
Confusion matrix for column foams considering frother type, excluding images in the same group for comparison.

	Confusion matrix			
DF250	112	0	0	42
MIBC	0	50	2	14
Octanol	0	0	87	23
PEG300	32	13	11	32

Classification accuracy: 67.2%

Table 6
Classes defined according to foam height.

Classes (H_f)	Conditions: Frother type (H_f)
16–18 cm	Octanol (16 cm); PEG300 (16–17 cm); MIBC (18 cm)
22–24 cm	DF250, MIBC and Octanol (22 cm); PEG300 (24 cm)
26–29 cm	MIBC (26 cm); Octanol (26–29 cm); DF250 (27 cm)
⩾36 cm	DF250 (36–62 cm)

Table 7
Confusion matrix for column foams considering foam height, excluding images in the same group for comparison.

	Confusion matrix			
H_f: 16–18 cm	16	35	25	12
H_f: 22–24 cm	44	4	24	16
H_f: 26–29 cm	20	47	21	0
H_f: ⩾36 cm	39	7	0	42

Classification accuracy: 23.6%

Table 8
Classes defined according to foam gas holdup.

Classes ($\hat{\varepsilon}_{gf}$)	Conditions: Frother type (H_f)
~52%	MIBC (18 cm); Octanol (16 cm)
~56%	PEG300 (16 cm); Octanol (19 cm)
~58%	PEG300 (17 cm); Octanol (22 cm)
~63%	MIBC (26 cm); Octanol (29 cm)
~68%	DF250 (27 cm); PEG300 (24 cm)

Table 9
Confusion matrix for column foams considering foam gas holdup, excluding images in the same group for comparison.

	Confusion matrix				
$\hat{\varepsilon}_{gf} \sim 52\%$	0	30	2	12	0
$\hat{\varepsilon}_{gf} \sim 56\%$	18	1	0	1	24
$\hat{\varepsilon}_{gf} \sim 58\%$	5	0	8	0	31
$\hat{\varepsilon}_{gf} \sim 63\%$	29	12	2	0	1
$\hat{\varepsilon}_{gf} \sim 68\%$	0	23	21	0	0

Classification accuracy: 4.1%

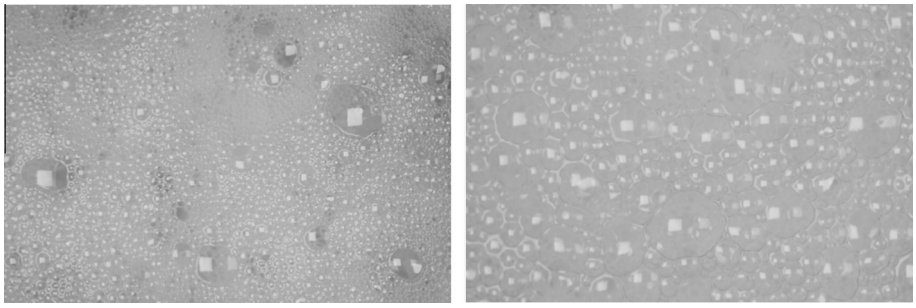

Fig. 11. Foams with $\widehat{\varepsilon}_{g,f}$ = 63% generated with MIBC at H_f = 23 cm (left), and Octanol at H_f = 29 cm (right).

on the height relative to the maximum foam height achievable with the reagent being tested. For instance, it cannot be expected that a 26–27 cm of foam generated with DF250 behave in the same way as 26–27 cm of foam generated with MIBC, because the latter corresponds to the maximum height achievable with MIBC, while DF250 can generate twice as much foam in the same system. It is interesting to notice that the classification accuracy of a random classification would be around 25%, so foam height cannot be considered to define foam texture.

Finally, the last way of grouping the foam images, is by foam gas holdup. This is done in Table 8 for $\widehat{\varepsilon}_{g,f}$ ranging between 52% and 68%. To avoid the generation of too many classes, the images generated at the highest values of foam height with DF250 were not considered.

The result of comparing and classifying the foam images according to foam gas holdup is presented in Table 9. The images corresponding to the same conditions of foam gas holdup and frother type were excluded from the comparison step when applying the variogram-based textural classification.

The results show a classification accuracy of 4.1%, i.e., more than 95% of images are misclassified when the foam gas holdup is considered to generate the classes. This means that even though the foam gas holdup may be the same, textures differ depending on frother type and/or foam height. This can be confirmed directly from the foam images, as it can be seen in Fig. 11, where foams with the same $\widehat{\varepsilon}_{g,f}$ are presented.

Fig. 11 shows foam images generated with different frothers, at different foam heights, but with the same foam gas holdup (63%). The image on the left corresponds to MIBC at H_f = 23 cm, and the image on the right corresponds to Octanol at H_f = 29 cm. In this case, the difference in texture can be easily detected with the naked eye.

4. Conclusions

A variogram-based technique to compare and classify foams according to their texture was introduced. The technique was used with two sets of images, corresponding to foams generated in a quasi-2D cell and in a laboratory column. In the case of the quasi-2D foams, even though the bubble size distribution in the images did not show a significant variation between frothers, the textures generated with Oreprep F549, MIBC and Octanol were recognised as different by the variogram-based textural classification algorithm, with a classification accuracy of 88.9%. In the case of the foam images generated in the laboratory column, three sets of classes were generated, corresponding to frother type, foam height and foam gas houldup. The results suggest that foam texture is mainly defined by froth type, with some effect of foam height. The column foam images did not show similar characteristics when grouped by foam gas holdup, which was confirmed with the variogram-based technique. The classification accuracy in this case was lower than 5%, showing that foam texture in the column was not determined by foam gas holdup.

Acknowledgements

The laboratory column tests were performed at McGill University, and the authors would like to thank the Mining and Materials Engineering Department, and Dr. Cesar Gomez for his support. The authors acknowledge the Chilean National Commission for Scientific and Technological Research (CONICYT) for funding this research through the Basal Financing Program FB0809, and Universidad de Chile for supporting the stay of D. Mesa at McGill University to perform part of the experiments. This work made use of the free software package GNU Octave, and the authors are grateful for the support of the Octave development community.

References

Aldrich, C., Marais, C., Shean, B., Cilliers, J., 2010. Online monitoring and control of froth flotation systems with machine vision: a review. Int. J. Miner. Process. 96 (1), 1–13.
Atkinson, P.M., Lewis, P., 2000. Geostatistical classification for remote sensing: an introduction. Comput. Geosci. 26 (4), 361–371.
Barbian, N., Hadler, K., Ventura-Medina, E., Cilliers, J., 2005. The froth stability column: linking froth stability and flotation performance. Miner. Eng. 18 (3), 317–324.
Barnes, R., 2003. Variogram Tutorial. Golden. Software, Golden, CO. Available online at http://www.goldensoftware.com/variogramTutorial.pdf.
Bartolacci, G., Pelletier, P., Tessier, J., Duchesne, C., Bossé, P.-A., Fournier, J., 2006. Application of numerical image analysis to process diagnosis and physical parameter measurement in mineral processes – part I: flotation control based on froth textural characteristics. Miner. Eng. 19 (6), 734–747.
Bonetto, R., Ladaga, J., 1998. The variogram method for characterization of scanning electron microscopy images. Scanning 20 (6), 457–463.
Bonifazi, G., Serranti, S., Volpe, F., Zuco, R., 2001. Characterisation of flotation froth colour and structure by machine vision. Comput. Geosci. 27 (9), 1111–1117.
Carr, J.R., De Miranda, F.P., 1998. The semivariogram in comparison to the co-occurrence matrix for classification of image texture. IEEE Trans. Geosci. Remote Sens. 36 (6), 1945–1952.
Chica-Olmo, M., Abarca-Hernandez, F., 2000. Computing geostatistical image texture for remotely sensed data classification. Comput. Geosci. 26 (4), 373–383.
Deutsch, C., Journel, A., 1997. GSLIB: Geostatistical Software Library and User's Guide. Oxford University Press.
Emery, X., Kracht, W., Egaña, Á., Garrido, F., 2012. Using two-point set statistics to estimate the diameter distribution in boolean models with circular grains. Math. Geosci. 44 (7), 805–822.
Finch, J.A., Nesset, J.E., Acuña, C., 2008. Role of frother on bubble production and behaviour in flotation. Miner. Eng. 21 (12), 949–957.
Fotsing, J., Tonye, E., Zobo, B., Saley, M., Kouame, F., et al., 2013. Characterization of the texture of digital Images by variography approach: an application to the classification of SAR images. Geoinformatics Geostatistics: Overview S1 (6), 2.
Hadler, K., Cilliers, J., 2009. The relationship between the peak in air recovery and flotation bank performance. Miner. Eng. 22 (5), 451–455.
Holtham, P., Nguyen, K., 2002. On-line analysis of froth surface in coal and mineral flotation using JKFrothCam. Int. J. Miner. Process. 64 (2), 163–180.
Jakomulska, A., Clarke, K., 2001. Variogram-derived measures of textural image classification. In: geoENV III-Geostatistics for Environmental Applications. Springer, pp. 345–355.
Kracht, W., Emery, X., Paredes, C., 2013. A stochastic approach for measuring bubble size distribution via image analysis. Int. J. Miner. Process. 121, 6–11.

Li, R., Wraith, A., Harris, R., 1994. Gas dispersion phenomena at a narrow slot submerged in a liquid. Chem. Eng. Sci. 49 (4), 531–540.
Moolman, D., Aldrich, C., Van Deventer, J., Bradshaw, D., 1995a. The interpretation of flotation froth surfaces by using digital image analysis and neural networks. Chem. Eng. Sci. 50 (22), 3501–3513.
Moolman, D., Aldrich, C., Van Deventer, J., Stange, W., 1995b. The classification of froth structures in a copper flotation plant by means of a neural net. Int. J. Miner. Process. 43 (3), 193–208.
Tsatouhas, G., Grano, S., Vera, M., 2006. Case studies on the performance and characterisation of the froth phase in industrial flotation circuits. Miner. Eng. 19 (6), 774–783.
Tuceryan, M., Jain, A.K., 1998. The Handbook of Pattern Recognition and Computer Vision. World Scientific Publishing Co., pp. 207–248 (Chapter Texture Analysis).
Woodcock, C.E., Strahler, A.H., Jupp, D.L., 1988a. The use of variograms in remote sensing: I. Scene models and simulated images. Remote Sens. Environ. 25 (3), 323–348.
Woodcock, C.E., Strahler, A.H., Jupp, D.L., 1988b. The use of variograms in remote sensing: II. Real digital images. Remote Sens. Environ. 25 (3), 349–379.
Wu, S.-s., Xu, B., Wang, L., 2006. Urban land-use classification using variogram-based analysis with an aerial photograph. Photogramm. Eng. Remote Sens. 72 (7), 813–822.